10-17-2008

Seasonal variations of semidiurnal tidalperturbations in mesopause region temperature and zonal and meridional winds above Fort Collins, Colorado(40.6°N, 105.1°W)

Titus Yuan
Utah State University

H. Schmidt

C. Y. She

D. A. Krueger

S. Reising

Recommended Citation
Yuan, T., H. Schmidt, C. Y. She, D. A. Krueger, and S. Reising (2008), Seasonal variations of semidiurnal tidal perturbations in mesopause region temperature and zonal and meridional winds above Fort Collins, Colorado (40.6°N, 105.1°W), J. Geophys. Res., 113, D20103, doi:10.1029/2007JD009687.

Seasonal variations of semidiurnal tidal perturbations in mesopause region temperature and zonal and meridional winds above Fort Collins, Colorado (40.6°N, 105.1°W)

Tao Yuan,[1,2] Hauke Schmidt,[3] C. Y. She,[1] David A. Krueger,[1] and Steven Reising[2]

Received 7 December 2007; revised 9 July 2008; accepted 18 July 2008; published 17 October 2008.

[1] On the basis of Colorado State University (CSU) Na lidar observations over full diurnal cycles from May 2002 to April 2006, a harmonic analysis was performed to extract semidiurnal perturbations in mesopause region temperature and zonal and meridional winds over Fort Collins, Colorado (40.6°N, 105.1°W). The observed monthly results are in good agreement with MF radar tidal climatology for Urbana, Illinois, and with predictions of the Hamburg Model of the Neutral and Ionized Atmosphere (HAMMONIA), sampled at the CSU Na lidar coordinates. The observed semidiurnal tidal period perturbation within the mesopause region is found to be dominated by propagating modes in winter and equinoctial months with a combined vertical wavelength varying from 50 km to almost 90 km and by a mode with evanescent behavior and longer vertical wavelength (100–150 km) in summer months, most likely due to dominance of (2, 2) and (2, 3) tidal (Hough) modes. The observed semidiurnal tidal amplitude shows strong seasonal variation, with a large amplitude during the winter months, with a higher growth rate above ~85–90 km, and minimal amplitudes during the summer months. Maximum tidal amplitudes over 50 m/s for wind and 12 K for temperature occur during fall equinox. A detailed comparison with HAMMONIA predictions shows excellent agreement in semidiurnal phases. HAMMONIA-predicted semidiurnal amplitudes generally agree well with observations; however, HOMMONIA underestimates temperature amplitudes in some of the nonsummer months as well as zonal wind and meridional wind amplitudes in April and September but overestimates them in February. To reveal the effects of the atmospheric background on vertical propagation of tidal modes and their relative importance in the composite semidiurnal tide during different seasons, we use the lidar-observed monthly mean temperature and zonal wind from the same data set as well as HAMMONIA output to calculate the vertical wave number seasonal variations of the major tidal modes of the migrating semidiurnal tide. This leads to a qualitative understanding of the lidar-observed and HAMMONIA-predicted seasonal variation of the semidiurnal tidal perturbation.

Citation: Yuan, T., H. Schmidt, C. Y. She, D. A. Krueger, and S. Reising (2008), Seasonal variations of semidiurnal tidal perturbations in mesopause region temperature and zonal and meridional winds above Fort Collins, Colorado (40.6°N, 105.1°W), *J. Geophys. Res.*, *113*, D20103, doi:10.1029/2007JD009687.

1. Introduction

[2] Solar thermal tides are global-scale waves that dominate the dynamical motion in the mesosphere and lower thermosphere (MLT) because their amplitude grows with altitude to conserve wave energy. When propagating into the MLT region, the horizontal wind tidal amplitude can reach the magnitude of the mean wind. While the diurnal tide tends to be confined equatorward of 30°, the semidiurnal tide reaches its peak amplitude in the midlatitudes [*Forbes*, 1982b, 1995; *Vincent et al.*, 1989; *Manson et al.*, 1989; *Manson and Meek*, 1991]. The location of the Colorado State University Na lidar at Fort Collins, Colorado (40.6°N, 105.1°W), and mesopause region (80–110 km) coverage, along with fluorescence lidar's advantages of high temporal and spatial resolution and the capability of full diurnal cycle simultaneous observation of temperature and horizontal wind, provide a unique opportunity to study tidal perturbations and their variability [*She*, 2004; *She et al.*, 2004].

[3] At a single longitude, one may observe local oscillations at harmonics of the diurnal frequency but not be able to determine whether these oscillations are global (migrat-

[1]Department of Physics, Colorado State University, Fort Collins, Colorado, USA.
[2]Department of Electrical and Computer Engineering, Colorado State University, Fort Collins, Colorado, USA.
[3]Max Planck Institute for Meteorology, Hamburg, Germany.

0148-0227/08/2007JD009687

ing or nonmigrating), local, or superposition of the two. The characteristics of solar tidal waves may be deduced either from zonally averaged local time observations at multiple longitudes that cover full diurnal cycles or from a combination of satellite observations, providing partial local time global coverage, and ground-based full diurnal cycle observations at a fixed location. However, both of these opportunities for joint observation are rare. The semidiurnal tidal period perturbations, reported in this paper, are considered to be monthly means, each computed from about 10 days of full diurnal cycle observations. This amount of data is necessary to average out the variability due to interactions with gravity waves (GWs) and modulation by mean state variation and by short-period planetary waves (PWs) (e.g., 2-day and 5-day waves), leaving only the prevailing tidal periods of interest. Such data are the closest observational representation of solar tides at one location, including both migrating and nonmigrating components, both of which are essential for the evaluation of global models. The seasonal variations of the diurnal tidal period perturbations, which are dominated by the migrating solar thermal tide, in temperature and zonal and meridional winds in the mesopause region over Fort Collins were reported on the basis of the data set from 2002 to 2003 [*Yuan et al.*, 2006]. This paper will focus on the semidiurnal tidal perturbation in these three thermodynamic variables, on the basis of an extended observation period from May 2002 to April 2006.

[4] The factors that contribute to the semidiurnal tidal variations in the MLT include (1) tidal forcing in the troposphere and stratosphere, mainly H_2O and O_3 absorption of solar radiation [*Forbes*, 1995], as well as latent heat release due to raindrop formation [*Hagan and Forbes*, 2003], (2) modification of the propagation of semidiurnal tidal modes by vertical profiles of temperature and zonal wind, that is, so-called refractive effects [*Forbes and Vincent*, 1989; *Riggin et al.*, 2003], (3) "mode coupling" resulting from the nonlinear effects of background mean zonal wind and the meridional temperature gradient on the tidal vertical propagation [*Lindzen and Hong*, 1974; *Walterscheid et al.*, 1980], and (4) nonlinear interactions between PWs and migrating tides [*Beard et al.*, 1999]. There is no significant tidal source in the mesopause region, except for in situ forcing due to chemical [*Mlynczak and Solomon*, 1993] and secondary ozone heating [*Thomas*, 1990], which is not as significant as the semidiurnal tidal forcing from the troposphere and stratosphere [*Hagan*, 1996]. Eddy diffusion due to GW saturation and its related energy dissipation should have a much less significant influence on the semidiurnal tide than it has on the diurnal tide, owing to the longer vertical wavelength (fast vertical propagation) of the semidiurnal tide [*Forbes*, 1982a], with the exception of higher-order modes such as (2, 5) and (2, 6).

[5] There have been many tidal studies of horizontal winds in the mesopause region based on ground-based radar observations [*Tsuda et al.*, 1988; *Vincent et al.*, 1989; *Manson et al.*, 1989; *Avery et al.*, 1989; *Franke and Thorsen*, 1993]. Although relative temperature measurements are possible with meteor radar [*Tsutsumi et al.*, 1996; *Hocking et al.*, 1997], studies of tidal temperature variations from radar observations have been rare. Temperature measurements with high spatial resolution in the mesopause region are ed routinely by sodium and potassium lidars, but they are currently generally limited to nighttime conditions at this juncture. Although they suffer from aliasing due to gaps in the data, the amplitude and phase of the semidiurnal temperature tides have been well determined using multinight observations made over the course of many hours each night [*Williams et al.*, 1998]. Daytime temperature measurements with sodium lidar have been possible since 1995 [*Chen et al.*, 1996] and more recently with potassium lidar [*Fricke-Begemann et al.*, 2002], enabling the determination of temperature diurnal tidal period oscillation based on full diurnal cycle observations in the mesopause region. To date, the only two sets of diurnal data with yearlong coverage have led to published studies on seasonal variations of diurnal and semidiurnal temperature tides [*States and Gardner*, 2000; *She et al.*, 2002]. Since May 2002, regular full diurnal cycle observations of mesopause region temperature and zonal and meridional winds have been conducted at Colorado State University. By April 2006, the combined data set consisted of 120 full diurnal cycles distributed throughout the year, with a minimum of 7 cycles in April and a maximum of 18 cycles in August. The reported seasonal variations of diurnal tides based on 2002–2003 data [*Yuan et al.*, 2006] are in qualitative agreement with those deduced from the full data set. Earlier comparisons of model results with observations [*Forbes and Vial*, 1989; *Pancheva et al.*, 2002], coupled with diagnostic studies involving thermosphere-ionosphere-mesosphere-electrodynamics general circulation model (TIME-GCM) [*Roble*, 2000] and the Global Scale Wave Model (GSWM) [*Hagan et al.*, 1999; *Hagan and Roble*, 2001], provided new insight into the behavior and impact of tides and PW in the MLT region. Our initial comparisons [*She et al.*, 2004; *Yuan*, 2004] of lidar-observed tides with GSWM predictions indicated that while there is general agreement in diurnal tides, the model prediction typically underestimated the semidiurnal amplitudes during the nonwinter months. This discrepancy was also reported in an earlier comparison with radar winds [*Pancheva et al.*, 2002] at different longitudes. In this paper, the seasonal variation of semidiurnal tides in temperature and zonal and meridional winds will be compared to the local output at 41.0°N, 105.0°W of the Hamburg Model of the Neutral and Ionized Atmosphere (HAMMONIA) [*Schmidt et al.*, 2006], a chemistry climate model of the atmosphere from the surface to about 250 km. Since this model includes (either explicitly or implicitly) all processes that are supposed to contribute to the tidal variability in the MLT region, and in particular full tropospheric chemistry and dynamics, a realistic prediction of tidal behavior can be expected. Comparisons of observed tide-removed mesopause mean fields (temperature and zonal and meridional winds) with HAMMONIA simulations based on the same data set were performed by *Yuan et al.* [2008]. A detailed assessment of the temporal data distribution and measurement accuracy are also presented therein.

2. Seasonal Variations of Semidiurnal Tides

[6] In this section, we discuss the seasonal variation of the temperature semidiurnal tide, followed by that of the zonal and meridional wind of the semidiurnal tide. Finally, we compare our zonal and meridional wind tidal results

Table 1. Equivalent Depths and Isothermal Vertical Wavelengths at 256 K and 200 K of Major Semidiurnal Tidal Modes[a]

Semidiurnal Tidal Mode	Equivalent Depth (km)	Vertical Wavelength (km)		m or $\|m\|$ (km^{-1})	
		256 K	200 K	256 K	200 K
(2, 2)	7.85	311.0	Evanescent	0.020	0.034
(2, 3)	3.67	81.4	83.0	0.077	0.076
(2, 4)	2.11	53.8	50.8	0.117	0.123
(2, 5)	1.37	41.0	37.9	0.153	0.166
(2, 6)	0.957	33.4	30.5	0.188	0.206

[a]The equivalent depth and vertical wavelength for 200 K are from *Forbes* [1995].

with the Urbana MF radar climatology (40.1°N, 88.2°W). The monthly amplitudes and phases of semidiurnal tidal period perturbations from the local output of HAMMONIA are deduced from temperature as well as zonal and meridional wind profiles at 3-h intervals for 3 years that were arbitrarily chosen from the simulation to represent present-day solar minimum conditions, as described by *Schmidt et al.* [2006]. This is done by using the same least squares fitting algorithm as for the lidar results. The locally observed semidiurnal tide is a superposition of the major migrating tidal modes (2, 2), (2, 3), (2, 4), (2, 5), and (2, 6), listed in Table 1, each with different vertical phase structure, plus nonmigrating tides, with the former dominating the latter. Migrating tides in temperature, zonal and meridional wind each have their own combination of these Hough modes. Therefore, we do not expect their vertical profiles to be identical. However, if one compares the observed phase structure of the three components (temperature and zonal and meridional winds) month by month, one finds considerable similarity in the slope of the three components' phase profiles, suggesting that one particular combination of Hough modes is the major contributor to all three. Generally, we observe that above ~85 km, the average vertical wavelength is shorter in winter (~50 km) and longer in summer (100–150 km), with intermediate equinoctial values in between (80–90 km), except in March when its average vertical wavelength is about 30 km.

2.1. Temperature Semidiurnal Tide

[7] Figure 1 shows the seasonal variations of temperature semidiurnal tidal amplitude (Figure 1, top) and phase (Figure 1, bottom) throughout the year. The tidal amplitude in December reaches its maximum of over 12 K near the top of the altitude range (100 km). For the equinoctial periods of February–March and September–October, the observed amplitudes are larger than model predictions in the intermediate altitude range of ~85–97 km, indicating a semiannual modulation. For example, at 90 km, HAMMONIA

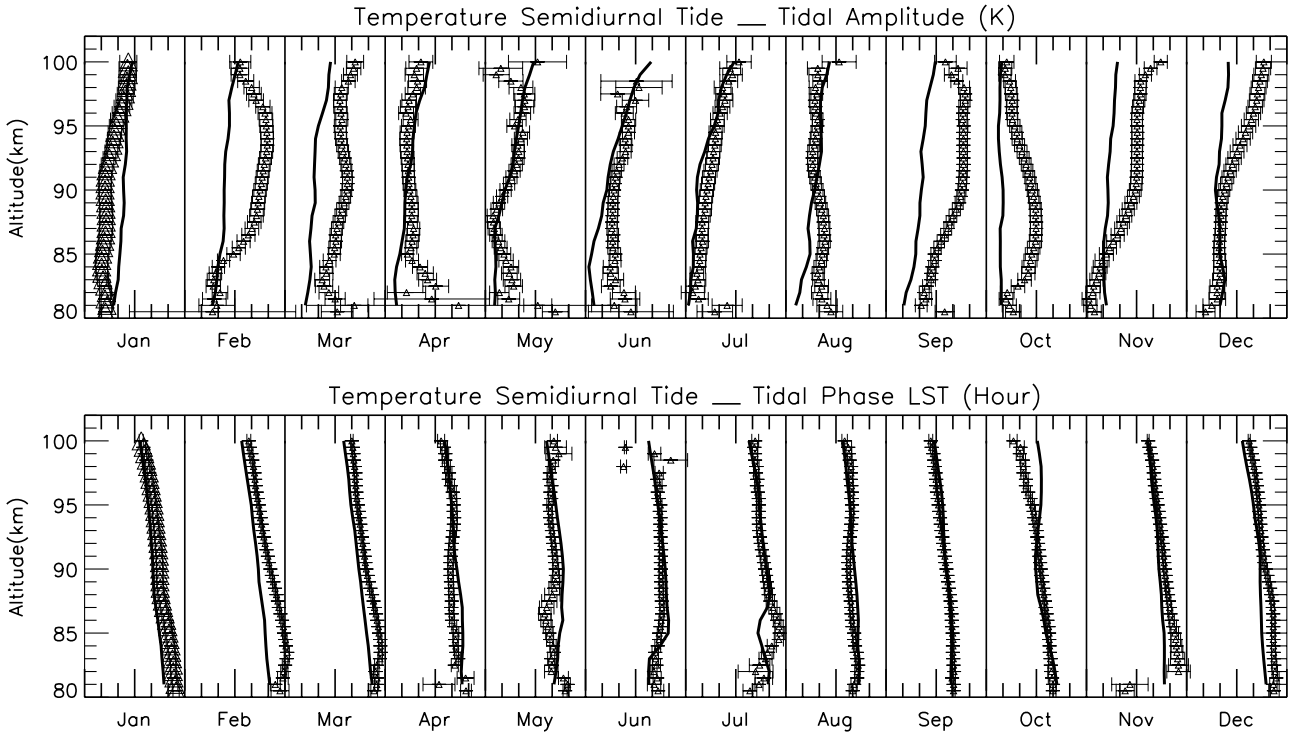

Figure 1. Temperature semidiurnal tidal (top) amplitude and (bottom) phase profiles for each month of the year measured by Na lidar (triangles with error bars) and HAMMONIA (solid lines). Each amplitude scale (horizont s) is 0–15 K, and each phase scale (horizontal axis) is 0–18 h.

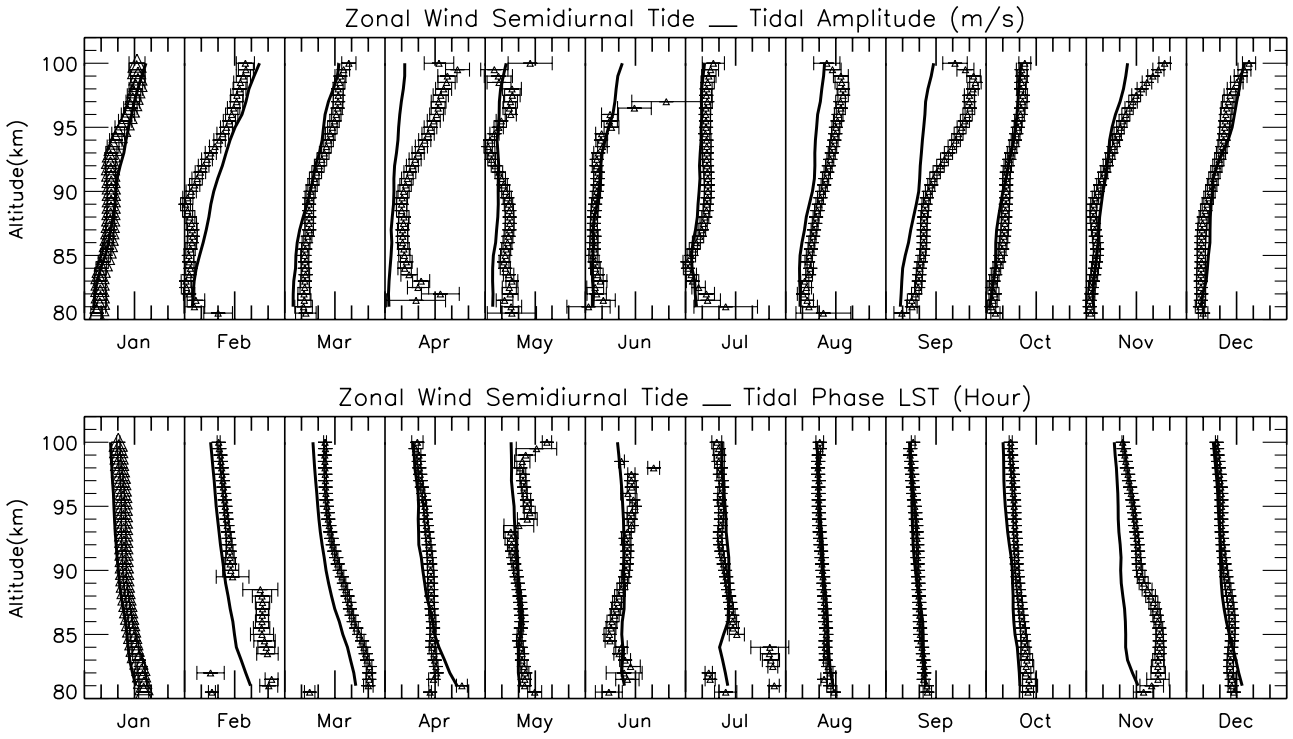

Figure 2. Same as Figure 1, except for zonal wind. Each amplitude scale (horizontal axis) is 0–60 m/s.

output is only half of the lidar results in February–March and September–November. During the other 7 months, the HAMMONIA model's semidiurnal tidal temperature amplitudes are in good agreement with lidar observations. Although semiannual modulation is normally an equatorial phenomenon [*Clancy et al.*, 1994], we reported previously its observation in semidiurnal tidal temperature amplitudes in midlatitudes [*She et al.*, 1995]. The amplitude enhancements in both equinoctial periods behave very similarly; the tidal amplitude grows rapidly from 80 to 88 km. It maintains an amplitude of over 10 K up to about 96 km and then decreases with height, approaching the model value at higher altitudes. The rapid rate of increase above this altitude in the observed temperature amplitudes is similar to those in the observed and predicted semidiurnal tidal wind amplitudes.

[8] The model predictions of semidiurnal temperature phase are in excellent general agreement (within 3 h, a quarter of the tidal period) for all months. The most noticeable feature of the temperature phase profiles is the downward phase progression with over 50-km vertical wavelength during most of the year, with the exception of the summer months. In June, the tidal phase is almost independent of altitude, implying either an evanescent mode or a propagating mode with very long vertical wavelength. Although HAMMONIA output shows that the average vertical wavelength in June from 70 to 100 km is about 90 km altitude, the limit in Na lidar altitude coverage makes it difficult to determine the exact vertical wavelength. More specifically, the vertical range of Na lidar coverage is only about one twelfth and one third of the 311-km and 82-km vertical wavelengths of the (2, 2) and (2, 3) modes, respectively [*Forbes*, 1995], as given in Table 1. In July, however, the 45-km v wavelength between 85 and 90 km deduced by lidar has the character of a typical propagating mode. Its wavelength is much longer above ~90 km, consistent with the phase profiles of May and June.

2.2. Zonal Wind Semidiurnal Tide

[9] Figure 2 shows the seasonal variation of the zonal wind semidiurnal tide, exhibiting small amplitudes of 10–15 m/s and long vertical wavelengths of over 100 km during the summer (poor-quality data above 95 km exhibits an erroneously large amplitude), but large amplitudes of over 50 m/s and relatively short vertical wavelengths of about 45 km during the winter. Although the agreement between the lidar results and HAMMONIA predictions at 90 km is much better than for temperature (except for February), HAMMONIA considerably underestimates the zonal wind amplitude at 95 km in April and September by one third and one half of lidar results, respectively. Most of the tidal amplitude profiles follow a similar pattern to each other, increasing with altitude, except for May and July, with an oscillatory pattern with altitude.

[10] Lidar-observed zonal wind semidiurnal phase has similar seasonal variations to temperature, with longer vertical wavelengths during summer than during winter, in very good agreement with model output. For example, in June, the lidar-deduced phase structure is complex, with upward phase progression (downward group velocity) between 85 and 90 km, suggesting the presence of an overlying tidal heating source [*Yu et al.*, 1997]. Even here, the observation is within the 2σ error of the nearly evanescent mode prediction of the HAMMONIA model, which does not show upward phase progression. The June phase becomes evanescent (within the error bars) at about 90 km. The vertical wavelengths from August to October are quite

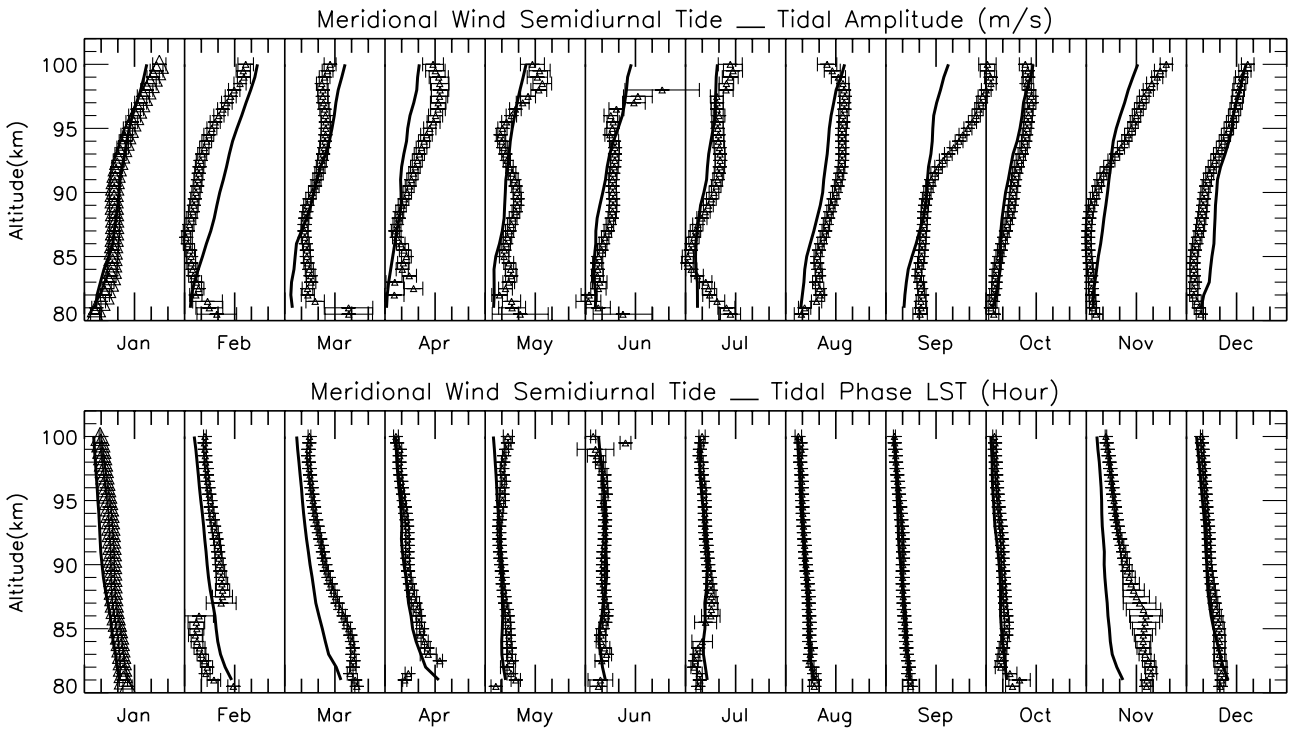

Figure 3. Same as Figure 2, except for meridional wind.

long as well, estimated to be over 90 km. The observed tidal phase progressions in November and December exhibit a transition at about 88 km altitude, where the semidiurnal tide changes from long vertical wavelength (almost constant phase progression) to shorter wavelengths (~50 km). The phase discontinuities observed below 90 and 85 km in February and July, respectively, are most likely due to weak tidal amplitudes of less than 10 m/s.

2.3. Meridional Wind Semidiurnal Tide

[11] As shown in Figure 3, the seasonal variations of the meridional wind semidiurnal tide are quite similar to those of the zonal wind semidiurnal tide, except for about 10 m/s larger amplitudes. Both wind components exhibit an oscillatory pattern with altitude in summer, especially in May. The meridional wind semidiurnal tidal phase is almost identical to the zonal wind semidiurnal tide, except that it leads by about 3 h, consistent with simple GW polarization relations. The observed polarization relations between each of the horizontal wind components and temperature are more complex than that between the zonal and meridional winds. In this case, though the meridional wind semidiurnal tides lead those of the zonal wind by 90°, the phase difference between zonal wind and temperature semidiurnal tides varies from 4 to 8 h for most of the mesopause region, depending on season and altitude.

[12] The semidiurnal tidal phase behavior in March is anomalous. The vertical wavelength increases from 25 to 50 km between 85 and 95 km. Above 95 km, the vertical wavelength increases dramatically (less evident in temperature semidiurnal phase). The average vertical wavelength is roughly ~30 km, very close to that of the high-order (2, 6) semidiurnal tidal mode, one of the least thermally excited semidiurnal tidal modes re unable to explain the phase structure in March simply by using linear theory. However, most of the phase profile in March is in agreement with the HAMMONIA prediction, so perhaps mode coupling effects and nonlinear interactions, as well as tide-GW [*Walterscheid*, 1981; *Fritts and Vincent*, 1987] and tide-PW [*Liu et al.*, 2007] interactions included implicitly in this general circulation model (GCM) can account for some of the observed anomalous behavior.

2.4. Comparison With Radar Wind Semidiurnal Tide for Urbana, Illinois

[13] Semidiurnal wind tides have been observed by MF radar [*Franke and Thorsen*, 1993; *Manson et al.*, 1999, 2004; *Riggin et al.*, 2003] for over a decade. The 2.66-MHz Urbana MF radar (40°N, 88°W) has been operating on a quasi-continuous basis since March 1991, yielding a climatology of zonal and meridional winds based on hourly means measurements from 1991 to 2000 with a vertical resolution of 3 km. Here, we compare lidar-observed horizontal wind semidiurnal tides to those of the 10-year climatology from Urbana MF radar measurements (available at http://soliton.csl.uiuc.edu/MFRadarSite/index.html). Differences between the two observations are expected, since they are from different longitudes (105.1°W versus 88.2°W), and cover different periods (2002–2006 versus 1991–2000). However, the two data sets show very similar seasonal variations. We have compared zonal wind semidiurnal tidal amplitudes and phases observed by the two techniques at 87, 90, and 96 km. Since the results between 87 and 90 km are essentially the same, we show only those at 90 and 96 km in Figures 4a and 4b and Figures 4c and 4d, respectively. The seasonal variation of semidiurnal tidal phase at either altitude shows very good agreement between the two experimental observations. At 90 km, the observed

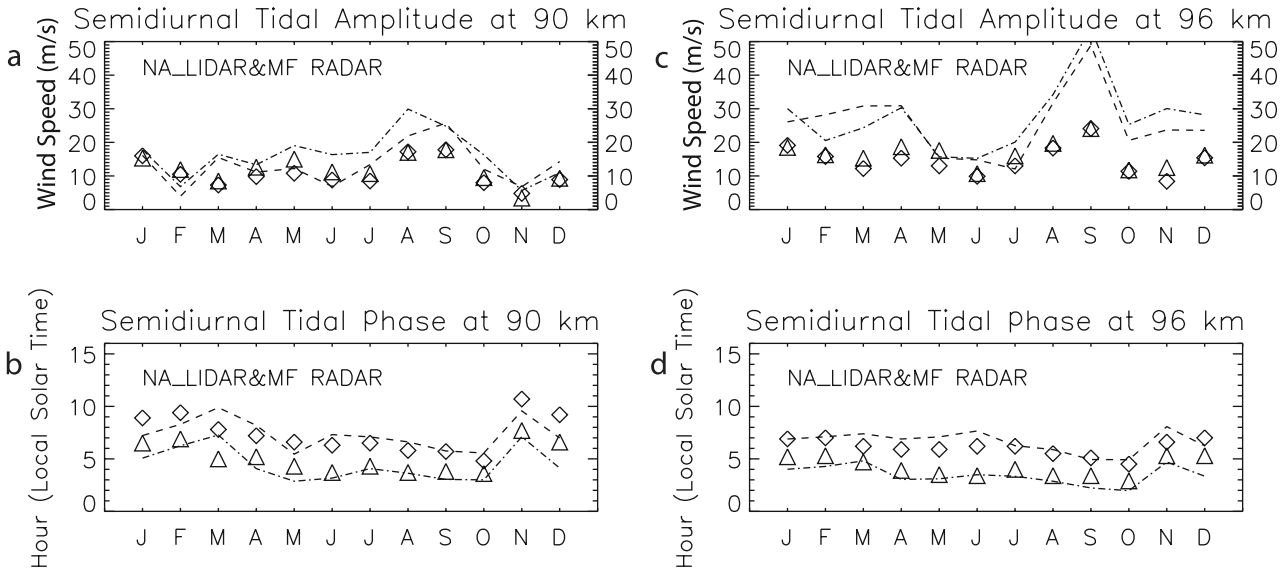

Figure 4. Semidiurnal tidal amplitude and phase comparison between the Colorado State University Na lidar-observed zonal wind (dashed line) and meridional wind (dash-dotted line), and MF radar (Urbana, Illinois) observed zonal wind (diamonds) and meridional wind (triangles): (a and b) for 90 km and (c and d) for 96 km.

semidiurnal amplitudes show not only similar seasonal variations, but also similar values. At the higher altitude, 96 km, lidar and radar disagree in nonsummer months, especially in September, when the zonal wind semidiurnal tidal amplitude observed by lidar and radar are 50 m/s and 24 m/s, respectively. During the summer months, however, the differences between the two instruments are quite small at the two altitudes, with both around 10–15 m/s.

3. Discussion

3.1. HAMMONIA Predictions of Migrating and Nonmigrating Semidiurnal Tides

[14] The local tidal period perturbations deduced from a realistic global GCM, such as HAMMONIA, at the coordinates of the ground-based instrument are most suitable for comparison with observed tidal harmonics from monthly mean full diurnal cycle observations. Such a comparison based on least squares fitting harmonic analysis has been presented in section 2. However, to be able to distinguish the migrating and nonmigrating tidal contributions to the composite tide, a global view of tidal behavior is needed. Therefore, we performed a Fourier analysis of the complete 3-D HAMMONIA data set and deduced the amplitude and phase of every component at the semidiurnal period with zonal wave numbers from 0 to 6, both eastward and westward propagating. The migrating semidiurnal tide is the westward propagating component with wave number 2 (W2) that is itself composed of a number of semidiurnal tidal (Hough) modes. All other components are nonmigrating tides. Figure 5 shows simulated zonal wind tidal amplitudes at 41.0°N of the migrating component from Fourier analysis of the global field (asterisks) and of the composite semidiurnal tidal period harmonics (migrating and nonmigrating) obtained from the least squares fitting of the data at a single longitude (diamonds) as a function of altitude, which are the HAMMONIA outputs as in Figure 2. The comparison of the amplitudes confirms that the migrating W2 is the dominant semidiurnal tide in the mesopause region except in October, when the amplitude of the W2 component is considerably weaker than the amplitude of the composite tide, which indicates there are significant contributions from components other than W2. In fact, in October, the simulated nonmigrating, eastward propagating component with wave number 3 has an amplitude of similar size to that of W2. In the case of temperature, the migrating component is still the major semidiurnal tidal period modulation, but not as dominant as in the case of winds. For example, in April, June, and September, the temperature amplitude of HAMMONIA's migrating tidal component is considerably smaller than the amplitude of the composite tide (not shown). This analysis suggests that, at 41.0°N, the migrating tides generally dominate the local HAMMONIA semidiurnal tidal period perturbations and therefore also dominate the tidal amplitude and phase seasonal variations. Since observation and local HAMMONIA outputs are in general agreement, we conclude that this migrating component dominance in semidiurnal tide is generally true in the atmosphere.

3.2. Effects of Mean Temperature and Zonal Wind on the Vertical Propagation of Semidiurnal Tides

[15] As the analysis of observations and the model has shown, the semidiurnal tidal vertical wavelength is changing as a function not only of altitude but also of seasons. This is likely due to the fact that different migrating semidiurnal tidal Hough modes, which have different vertical wavelengths (Table 1), are dominant in different months and at different altitudes. For example, the very long vertical wavelength during the summer implies dominance of the (2, 2) and (2, 3) modes, whereas the short vertical wavelength during the winter indicates a possible (2, 4) mode dominance. Although such information is

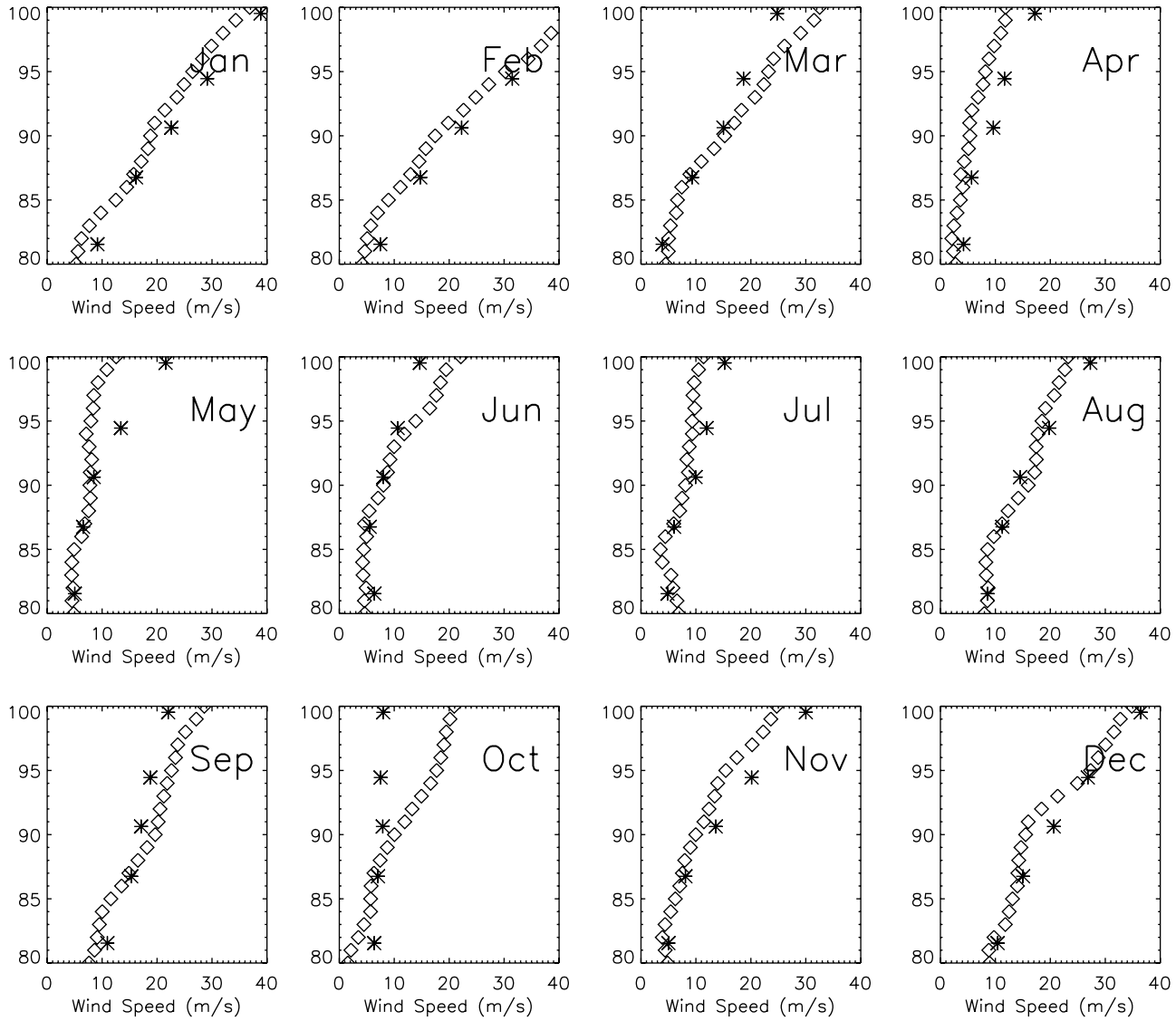

Figure 5. Comparison between zonal wind tidal amplitude of the migrating component (asterisks) and the composite (migrating and nonmigrating) semidiurnal tidal period perturbations (diamonds) as a function of altitude for each month from HAMMONIA. The former is derived from the global 3-D data set and the latter from local HAMMONIA output.

contained (or buried) in any comprehensive general circulation model, a simple physical explanation accounting for the general behavior of the seasonal variations shown in Figures 1–3 would advance our understanding of semidiurnal tides.

[16] The major migrating semidiurnal tidal modes consist of both symmetric ((2, 2), (2, 4), and (2, 6)) and antisymmetric ((2, 3) and (2, 5)) modes in winter and summer, but mainly symmetric modes at the equinoxes. These modes are excited in the stratosphere and troposphere. Their relative strength of excitation is season-dependent [*Forbes and Garrett*, 1978; *Forbes*, 1995]. Once excited, these modes experience the same exponential growth rate (1/2H, with H being the local scale height) to compensate for the decrease in atmospheric density, with (2, 2) dominance at the excitation altitude. However, its vertical wave number m (and its wavelength, $\lambda_z = 2\pi/m$) varies with the vertical distance from its source. Such variation depends on the equivalent depth of the mode, background temperature, and zonal wind [*Hines*, 1974; *Forbes and Vincent*, 1989]. Equations (1a)–(1c) show this relationship:

$$m^2 = \frac{N^2}{gh'_n} - \frac{1}{4H^2} \tag{1a}$$

$$h'_n = h_n\left(1 + \frac{U}{C_{ph}}\right)^4 \tag{1b}$$

$$N^2 = \frac{g}{T}\left(\frac{dT}{dz} + \Gamma_d\right) \tag{1c}$$

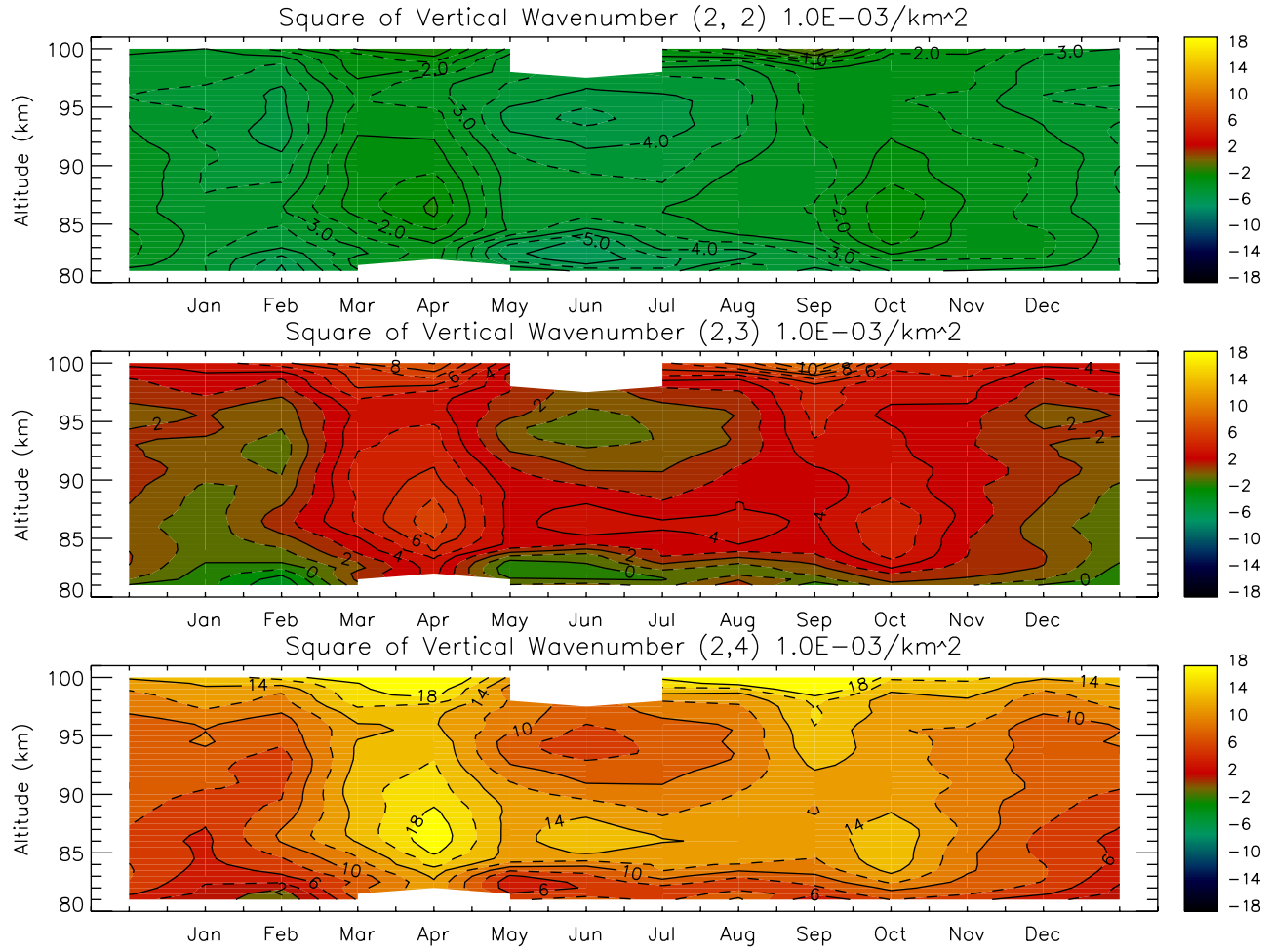

Figure 6. Square of the vertical wave number, m^2 of (top) the (2, 2) mode, (middle) the (2, 3) mode, and (bottom) the (2, 4) mode showing the effect of mean temperature and zonal wind taken from the Colorado State University Na lidar climatology.

where N and H are the Brunt-Vaisala frequency and the local scale height, respectively. Γ_d is the dry adiabatic lapse rate, which is about 9.5 K/km in the mesopause region. The equivalent depth of the tidal mode is h_n, denoted by the subscript n; its value and associated isothermal vertical wavelengths at 256 K and 200 K for the major semidiurnal tidal modes are given in Table 1 for the zero-wind situation. U is the zonal wind and C_{ph} is the horizontal phase velocity of the semidiurnal tide, which at 41.0°N, is about 350 m/s. If m^2 for a Hough mode becomes negative, the wave becomes evanescent (trapped) and its amplitude exponential growth rate is reduced by $|m|$ from the propagating mode value, $1/2H$. The altitude at which a Hough mode becomes evanescent is known as the switching altitude. So, it may happen that the dominant (2, 2) mode with the maximum thermal excitation becomes evanescent while the higher-order modes remain propagating [*Forbes*, 1995] within the MLT region. The (2, 2) mode, then, starts to lose its dominance over higher-order modes as it propagates upward from its switching altitude. Therefore, the altitude dependence of m^2 of the major tidal modes and their associated switching altitudes will determine whether individual modes are evanescent or propagating, in turn, determining the dominant character of the composite semidiurnal tide at a particular altitude.

[17] Our observations also provide a mean state climatology of temperature, zonal and meridional wind during the same data collection period [*Yuan et al.*, 2008]. By applying such observed monthly mean temperature, temperature gradient, and zonal wind to (1b) and (1c), we calculate m^2 for each month and each Hough mode and are therefore able to evaluate the effect of the background atmosphere on the vertical propagation of the migrating semidiurnal tide. Figure 6 shows the seasonal structure of m^2 for the (2, 2), (2, 3), and (2, 4) modes. The combined effect of temperature and wind cause m^2 of the (2, 2) mode to be negative between 80 and 100 km and thus evanescent in this region throughout the year, with its amplitude exponential growth rate reduced by $|m_{(2,2)}|$. In contrast to (2, 2), the m^2 of (2, 4) is positive throughout the year, and therefore its energy propagates upward into the mesopause region and above. The m^2 of (2, 3), on the other hand, is positive for most of the year, except for near the winter solstice below ~80 km and near the summer solstice above 95 km. On the basis of

HAMMONIA data, we have also evaluated the seasonal dependence of m^2 for these tidal modes below 80 km, and we found that, between 50 and 80 km, it is negative for the (2, 2) during all nonsummer months, but is less than zero only during the winter months for (2, 3). The m^2 of (2, 4) is positive throughout the year as it is in the mesopause region.

[18] Near the winter solstice, the major modes are excited in the troposphere and stratosphere. At ~50 km, the heating rate reaches its maximum [*Forbes and Garrett*, 1978]. The (2, 2) mode is dominant because of its maximum thermal excitation among all major modes, followed by (2, 3) and (2, 4) each with ~25% of the strength of the (2, 2) mode. As shown earlier, both (2, 2) and (2, 3) are evanescent (negative m^2) above the excitation altitude up as opposed to the (2, 4) mode, which propagates up to and beyond 100 km. Since the (2, 3) and (2, 4) modes are excited with comparable strength at ~50 km but the (2, 3) mode's amplitude exponential growth rate has a decay factor of $|m_{(2,3)}|$ at ~80 km, (2, 3) becomes negligible in relation to the (2, 4) mode. Here it is necessary to reiterate that (2, 3) will not be excited during the equinox since it is an asymmetric mode. Therefore, we understand the lidar-observed phase change in the mesopause region during nonsummer months by determining the growth of the (2, 2) and (2, 4) modes. Although the (2, 2) mode is about four times stronger than the (2, 4) modes at the excitation altitude, its growth rate is reduced by $|m^2_{(2,2)}| \sim 0.003\ \mathrm{km}^{-1}$, and it loses its dominance to (2, 4) mode that propagates above 90 km. Also, to a lesser extent, additional high-order modes, such as (2, 4) and (2, 5), can also be generated at the expense of the lower-order modes because of the ''mode coupling'' effect [*Lindzen and Hong*, 1974; *Walterscheid et al.*, 1980]. So the net effect is that in November and December, the vertical wavelength changes from a (2, 2) and (2, 3) value of ~100 km to a much smaller value of about 50 km, characteristic of the (2, 4) mode above ~90 km.

[19] Under summer solstice conditions, the excitation amplitude of the (2, 3) mode is about 40% that of the (2, 2) mode, followed by the (2, 4) and (2, 5) modes, each about 30% of that of the (2, 2) mode [*Forbes and Garrett*, 1978]. Though the decay factor, $|m_{(2,2)}|$, of amplitude growth rate in the mesopause region is comparable in summer and winter (Figure 6), the main difference lies in the wind structure below 80 km, where zonal winds are eastward during the winter and westward during the summer in the upper stratosphere and the mesosphere. Using the HAMMONIA data for the m^2 calculation mentioned above, the (2, 2) mode remains propagating (m^2 stays positive) up to ~75 km in June and ~80 km in July. The (2, 3) mode also remains propagating up to ~95 km. Therefore, during the summer, (2, 2) and (2, 3) experience the shortest decay distance from switching altitude throughout the year and become the dominant semidiurnal tidal modes, which leads to long vertical wavelength of the semidiurnal tides in summer.

[20] Near the equinoxes, the zonal wind is close to zero, leading to a (2, 2) switching altitude somewhere between that of the winter and summer solstice. Since the asymmetric (2, 3) and (2, 5) modes are hardly excited at the equinoxes, the (2, 4) and (2, 6) modes are excited with 40% and 25%, respectively, of the (2, 2) mode's strength [*Forbes and Garrett*, 1 One would expect the (2, 4) mode dominance at a lower altitude than that of winter. However, $|m^2_{(2,2)}|$ is smaller (only ~0.0015) near the equinoxes (Figure 6), which means the amplitude of the (2, 2) mode decays more slowly than during the summer and winter solstices. The net effect is that the (2, 2) mode is still dominant in a significant portion of the mesopause region and thus makes the average vertical wavelength 80–90 km.

[21] The seasonal variation of the semidiurnal tidal amplitude, as presented in Figures 1–3, is influenced by a number of factors, such as heating rates, refractive effects just discussed, and GW and PW interactions. A full quantitative discussion of the causes for the seasonal variation is beyond the scope of this paper. An example of how such a discussion can be attempted is given by *Achatz et al.* [2008], who used a combination of HAMMONIA and a linear model to study the origin of the diurnal tide's seasonal variation. The following qualitative discussion is intended to provide an overview of possible mechanisms contributing to the seasonal variation of the semidiurnal tidal amplitude and to motivate future work.

[22] To account for the tidal amplitude seasonal variations qualitatively, first, we discuss the seasonal dependence of excitation heating rate. *Hagan* [1996] discussed the comparative effects of migrating tidal sources in the troposphere and stratosphere that affect the MLT region, and pointed out that, during the summer, the 6-h phase difference between the infrared (H_2O) and ultraviolet (O_3 and O_2) heating could reduce the total thermal excitation of the semidiurnal tide. On the other hand, during the winter (and similarly in autumn), this phase difference is about 2 h and therefore the excitation of semidiurnal tidal amplitude increases. Therefore, the excitation alone could produce the basic seasonal variation of semidiurnal tidal amplitudes, with large amplitudes in winter and small amplitudes in summer, along with autumn amplitude enhancement larger than that of spring in semidiurnal tides. The HAMMONIA-deduced migrating tidal period heating rates (not shown) are both quantitatively and qualitatively similar to those presented by *Hagan* [1996]. Momentum conservation of a nondissipating wave requires its amplitude to be proportional to the square root of the vertical wave number before it reaches the saturation level [*Lindzen*, 1981; *Fritts*, 1984], that is, $|u'| \sim m^{1/2}$. This suggests that for equal excitation at a temperature of 200 K, for example, the perturbations of the (2, 4) mode would have 1.9 times the amplitude of the (2, 2) mode (Table 1), implying the tidal amplitude equinoctial enhancement, since the lidar observes a significant equinoctial peak in m^2 (Figure 6). The heating rate difference between autumn and spring [*Hagan*, 1966] is likely to cause higher amplitudes in autumn than in spring. In addition to the atmospheric refractive effect [*Riggin et al.*, 2003], the tide-PW interaction may also be a contributing factor to the early fall amplitude enhancement as discussed by *Smith et al.* [2007].

[23] Although it is difficult to assess quantitatively, we acknowledge that there is unequal dissipation of the major tidal modes contributing to the observed local harmonics at the semidiurnal tidal period. Since the molecular diffusion rate is low in the mesopause region, eddy diffusion, which depends on wave dynamics, would dominate the damping effect, especially near saturation, or the instability region. In theory, when viscosity becomes sufficiently large, the

exponential growth of a tidal mode could be retarded or could cease. Though there have been considerable discussions of the effect of eddy diffusion on the dominant (1, 1) diurnal tidal mode [*Forbes*, 1982a; *Forbes and Hagan*, 1988], the lack of discussion on this effect on the semidiurnal tidal modes is justifiable, principally due to the fact that the rate of wave energy dissipation for a given viscosity is proportional to the square of the vertical wave number of the wave [*Hines*, 1974; *Forbes and Vincent*, 1989]. Unlike the diurnal tidal modes, whose vertical wavelengths, λ_z, are shorter than ~30 km, the λ_z for the dominant semidiurnal tidal modes, (2, 2), (2, 3), and (2, 4), are respectively about 300, 80, and 50 km.

[24] In his seminal paper, *Hines* [1960] studied the damping of gravity waves by viscous dissipation. By equating the energy per unit mass of an internal gravity wave mode to the dissipation per unit mass over one wave period, $\tau = 2\pi/\omega$, and by invoking the dispersion relation, he derived a simple formula that relates kinematic viscosity, η, to the parameters of a wave mode, whose energy would be lost completely in one period because of viscous dissipation. For an isothermal atmosphere, this relation is $2\pi\eta k^2\omega_g^2 = \omega^3$ [*Hines*, 1960, equation (49)], where k, ω, and ω_g are, respectively, horizontal wave number, wave frequency, and isothermal Brunt-Vausala frequency. Using the dispersion relation, one may replace the horizontal wave number, k, by the vertical wave number, m, and obtain $2\pi\eta\, m^2 = \omega(1 - \omega^2/\omega_g^2)$ [*Beer*, 1974, equation (3.3.20)]. Applying this relationship to tidal waves, whose

$$\omega = \frac{2\pi}{\tau} \langle \langle \omega_g \approx 0.021 \text{ s}^{-1} (\text{at } 200 \text{ K}),$$

one can express a minimum vertical wavelength of a tidal wave as

$$\lambda_z = \frac{2\pi}{m} = 2\pi\sqrt{\tau\eta},$$

below which the tidal wave will presumably lose all its energy due to viscous dissipation in one wave period. For semidiurnal tide, τ = 43200 s, with typical molecular viscosity η(at 90 km) ≈ 4 m^2/s, $\lambda_{z,\min} \sim 2.6$ km. Even for a high eddy viscosity of ~500 m^2/s used in the literature [*Forbes*, 1982a], the deduced minimum vertical wavelength is $\lambda_{z,\min} \sim 30$ km. Indeed, this high value of eddy viscosity recently has been found to exist during the breaking of an internal gravity wave [*Li et al.*, 2007]. Since the vertical wavelengths of the major semidiurnal tidal modes (Table 1) are all longer than $\lambda_{z,\min}$, these modes should propagate without significant dissipation, even for high eddy viscosity, which is unlikely to be encountered by semidiurnal tide throughout the entire semidiurnal tidal period.

4. Summary and Conclusions

[25] Since May 2002, the CSU lidar group has performed full diurnal cycle observations of the mesopause region of the Earth's atmosphere. Observations between May 2002 and April 2006 have enabled the study of the seasonal variation of thermal tides over Fort Collins, Colorado. In this paper, we presented the li r-observed monthly semidiurnal tidal amplitudes and phases along with HAMMONIA output and MF radar data from Urbana, Illinois, showing good agreement among the three.

[26] Using the lidar-observed monthly mean temperature and mean zonal wind from the same data set and HAMMONIA output, we calculated the vertical wave number dependence of the major migrating semidiurnal tidal modes, from which we derived a qualitative understanding of the lidar-observed and HAMMONIA-predicted seasonal variation of the semidiurnal tides. Analysis based on HAMMONIA, lidar data, and early tidal theory [*Forbes and Garrett*, 1978] shows that it is the combination of seasonal variations of tidal thermal excitation and atmospheric mean fields that causes such "tidal mode selection" in the mesopause region. Therefore we correlated the seasonal variation of semidiurnal tidal vertical wavelength with different semidiurnal tidal mode dominance in different seasons at different altitude. This process led us to deduce the switching of dominance from the (2, 2) mode to the (2, 4) mode at ~90 km in winter, causing a corresponding change in vertical wavelength from exceeding 100 km, to a much shorter vertical wavelength of about 50 km at higher altitude. In summer months, the deduced dominance of the (2, 2) and (2, 3) modes leads to the long (100–150 km) vertical wavelength throughout the observed altitudes. Since the (2, 2) mode has smaller $|m^2_{(2,2)}|$ near the equinoxes than near the solstices, the amplitude decay is smaller, so the (2, 2) mode is still dominant in a significant portion of the mesopause region leading to the average vertical wavelength of 80–90 km.

[27] In conclusion, we found excellent agreement between observation and model prediction of semidiurnal tidal phases. The accompanying semidiurnal amplitudes exhibit different altitude dependence between summer and nonsummer months. In summer months (May–July) the amplitudes are weak but nearly constant with an oscillatory structure with altitude, while in nonsummer months, the amplitudes are large with greater growth rate above 85–90 km. The seasonal variation of the heating rate is most likely responsible for the larger semidiurnal tidal amplitude during the winter than during the summer. Such an explanation advances our qualitative understanding of the factors underlying the structure of semidiurnal tides. In the qualitative discussion, we suggested that because of their long vertical wavelengths, the dominating semidiurnal tidal modes are resilient to the eddy diffusion effect. However, the dissipation of a less important higher-order mode, for example, (2, 6) with $\lambda_z \sim 30$ km, which is comparable to the dominant diurnal tidal mode, (1, 1), may not be negligible. The significance of such dissipation and nonlinear interactions may be appreciated from the general agreement between observation and HAMMONIA predictions, which do include these effects.

[28] **Acknowledgments.** This work is supported in part by grants from the NASA (NAG5–13567 and NNX07AB64G) and from the National Science Foundation (ATM-0545221 and ATM-0335127). T.Y. and C.Y.S. thank Maura Hagan, Jeff Forbes, and Dave Fritts for helpful discussions. The simulations with HAMMONIA were performed at the German Climate Computing Center (DKRZ). HAMMONIA studies are supported by the Deutsche Forschungsgemeinschaft (DFG) within the CAWSES priority program. H.S. thanks Guy Brasseur for the opportunity to visit the National Center for Atmospheric Research (NCAR). This collaboration was initiated during his visit.

References

Achatz, U., N. Grieger, and H. Schmidt (2008), Mechanisms controlling the diurnal solar tide: Analysis using a GCM and a linear model, *J. Geophys. Res.*, *113*, A08303, doi:10.1029/2007JA012967.

Avery, S. K., et al. (1989), High latitude tidal behavior in the mesosphere and lower thermosphere, *J. Atmos. Terr. Phys.*, *51*, 595–608, doi:10.1016/0021-9169(89)90057-3.

Beard, A. G., N. J. Mitchell, P. J. S. Williams, and M. Kunitake (1999), Non-linear interactions between tides and planetary waves resulting in periodic tidal variability, *J. Atmos. Terr. Phys.*, *61*, 363–376, doi:10.1016/S1364-6826(99)00003-6.

Beer, T. (1974), *Atmospheric Wave*, pp. 103–104, Halsted, New York.

Chen, H., et al. (1996), Daytime mesopause temperature measurements using a sodium-vapor dispersive Faraday filter in lidar receive, *Opt. Lett.*, *21*, 1003–1005.

Clancy, R. T., D. W. Rusch, and M. T. Callan (1994), Temperature minima in the averaged thermal structure of the middle mesosphere (70–80 km) from analysis of 40–92 km SME global temperature profiles, *J. Geophys. Res.*, *99*, 19,001–19,020, doi:10.1029/94JD01681.

Forbes, J. M. (1982a), Atmospheric tides: 1. Model description and results for the solar diurnal component, *J. Geophys. Res.*, *87*, 5222–5240, doi:10.1029/JA087iA07p05222.

Forbes, J. M. (1982b), Atmospheric tides: 2. The solar and lunar semidiurnal components, *J. Geophys. Res.*, *87*, 5241–5252, doi:10.1029/JA087iA07p05241.

Forbes, J. M. (1995), Tidal and planetary waves, in *The Upper Mesosphere and Lower Thermosphere: A Review of Experiment and Theory*, *Geophys. Monogr. Ser.*, vol. 87, edited by R. M. Johnson and T. L. Killeen, pp. 67–87, AGU, Washington, D. C.

Forbes, J. M., and H. B. Garrett (1978), Thermal excitation of atmospheric tides due to insolation absorption by H_2O and O_3, *Geophys. Res. Lett.*, *5*, 1013–1016, doi:10.1029/GL005i012p01013.

Forbes, J. M., and M. E. Hagan (1988), Diurnal propagating tide in the presence of mean winds and dissipation: A numerical investigation, *Planet. Space Sci.*, *36*, 579–590, doi:10.1016/0032-0633(88)90027-X.

Forbes, J. M., and F. Vial (1989), Monthly simulations of the solar semidiurnal tide in the mesosphere and lower thermosphere, *J. Atmos. Terr. Phys.*, *51*, 649–661, doi:10.1016/0021-9169(89)90063-9.

Forbes, J. M., and R. A. Vincent (1989), Effects of mean winds and dissipation on the diurnal propagating tide: An analytic approach, *Planet. Space Sci.*, *37*, 197–209, doi:10.1016/0032-0633(89)90007-X.

Franke, S. J., and D. Thorsen (1993), Mean winds and tides in the upper middle atmosphere at Urbana (40°N, 88°W) during 1991–1992, *J. Geophys. Res.*, *98*, 18,607–18,615, doi:10.1029/93JD01840.

Fricke-Begemann, C., M. Alpers, and J. Hoffner (2002), Daylight rejection with a new receiver for potassium resonance temperature lidars, *Opt. Lett.*, *27*, 1932–1934, doi:10.1364/OL.27.001932.

Fritts, D. C. (1984), Gravity wave saturation in the middle atmosphere: A review of theory and observations, *Rev. Geophys. Space Phys.*, *22*, 275–308, doi:10.1029/RG022i003p00275.

Fritts, D. C., and R. A. Vincent (1987), Mesospheric momentum flux studies at Adelaide, Australia: Observations and a gravity wave–tidal interaction model, *J. Atmos. Sci.*, *44*, 605–619.

Hagan, M. E. (1996), Comparative effects of migrating solar sources on tidal signatures in the middle and upper atmosphere, *J. Geophys. Res.*, *101*(D16), 21,213–21,222, doi:10.1029/96JD01374.

Hagan, M. E., and J. M. Forbes (2003), Migrating and nonmigrating semidiurnal tides in the upper atmosphere excited by tropospheric latent heat release, *J. Geophys. Res.*, *108*(A2), 1062, doi:10.1029/2002JA009466.

Hagan, M. E., and R. G. Roble (2001), Modeling diurnal tidal variability with the National Center for Atmospheric Research thermosphere-ionosphere-mesosphere-electrodynamics general circulation model, *J. Geophys. Res.*, *106*(A11), 24,869–24,882, doi:10.1029/2001JA000057.

Hagan, M. E., et al. (1999), GSWM-98: Results for migrating solar tides, *J. Geophys. Res.*, *104*(A4), 6813–6828, doi:10.1029/1998JA900125.

Hines, C. O. (1960), Internal atmospheric gravity waves at ionospheric heights, *Can. J. Phys.*, *38*, 1441–1481.

Hines, C. O. (1974), Diurnal tide in the upper atmosphere, in *The Upper Atmosphere in Motion*, *Geophys. Monogr. Ser.*, vol. 18, edited by C. O. Hines, pp. 627–657, AGU, Washington, D. C.

Hocking, W. K., T. Thayaparan, and J. Jones (1997), Meteor decay times and their use in determining a diagnostic mesospheric temperature-pressure parameter: Methodology and one year of data, *Geophys. Res. Lett.*, *24*, 2977–2980, doi:10.1029/97GL03048.

Li, T., C.-Y. She, H.-L. Liu, and M. T. Montgomery (2007), Evidence of a gravity wave breaking event and the estimation of the wave characteristics from sodium lidar observation over Fort Collins, CO (41°N, 105°W), *Geophys. Res. Lett.*, *34*, L05815, doi:10.1029/2006GL028988.

Lindzen, R. S. (1981), Turbulence and stress owing to gravity wave and tidal breakdown, *J. Geophys. Res.*, *86*, 9707–9714, doi:10.1029/JC086iC10p09707.

Lindzen, R. S., and S. Hong (1974), Effects of mean winds and horizontal temperature gradients on solar and lunar semidiurnal tides in the atmosphere, *J. Atmos. Sci.*, *31*, 1421–1466, doi:10.1175/1520-0469(1974)031<1421:EOMWAH>2.0.CO;2.

Liu, H.-L., et al. (2007), Comparative study of short-term diurnal tidal variability, *J. Geophys. Res.*, *112*, D18108, doi:10.1029/2007JD008542.

Manson, A. H., and C. E. Meek (1991), Climatologies of mean winds and tides observed by medium frequency radars at Tromso (70°N) and Saskatoon (52°N) during 1987–1989, *Can. J. Phys.*, *69*, 900–975.

Manson, A. H., et al. (1989), Climatologies of semi-diurnal and diurnal tides in the middle atmosphere (70–110 km) at middle latitudes (40–50), *J. Atmos. Terr. Phys.*, *51*, 579–593, doi:10.1016/0021-9169(89)90056-1.

Manson, A. H., et al. (1999), Seasonal variations of the semi-diurnal and diurnal tides in the MLT: Multi-year MF radar observations from 2 to 70N, and the GSWM tidal model, *J. Atmos. Sol. Terr. Phys.*, *61*, 809–828, doi:10.1016/S1364-6826(99)00045-0.

Manson, A. H., C. E. Meek, C. M. Hall, S. Nozawa, N. J. Mitchell, D. Pancheva, W. Singer, and P. Hoffmann (2004), Mesopause dynamics from the Scandinavian triangle of radars within the PSMOS-DATAR Project, *Ann. Geophys.*, *22*, 367–386.

Mlynczak, M. G., and S. Solomon (1993), A detailed evaluation of heating efficiency in the middle atmosphere, *J. Geophys. Res.*, *98*(D6), 10,517–10,541, doi:10.1029/93JD00315.

Pancheva, D., et al. (2002), Global-scale tidal structure in the mesosphere and lower thermosphere during PSMOS campaign of June–August 1999 and comparison with the global-scale wave model, *J. Atmos. Sol. Terr. Phys.*, *64*, 1011–1035, doi:10.1016/S1364-6826(02)00054-8.

Riggin, D. M., et al. (2003), MF radar observations of seasonal variability of semidiurnal motions in the mesosphere at high northern and southern latitudes, *J. Atmos. Sol. Terr. Phys.*, *65*, 483–493, doi:10.1016/S1364-6826(02)00340-1.

Roble, R. G. (2000), On the feasibility of developing a global atmospheric model extending from the ground to the exosphere, in *Atmospheric Science Across the Stratopause*, *Geophys. Monogr. Ser.*, vol. 123, edited by D. E. Siskind, S. D. Eckermann, and M. E. Summers, pp. 53–67, AGU, Washington, D. C.

Schmidt, H., et al. (2006), The HAMMONIA Chemistry Climate Model: Sensitivity of the mesopause region to the 11-year solar cycle and CO_2 doubling, *J. Clim.*, *19*, 3903–3931, doi:10.1175/JCLI3829.1.

She, C. Y. (2004), Initial full-diurnal-cycle mesopause region lidar observations: Diurnal-means and tidal perturbations of temperature and winds over Fort Collins, CO (41N, 105W), PSMOS 2002, *J. Atmos. Sol. Terr. Phys.*, *66*, 663–674, doi:10.1016/j.jastp.2004.01.037.

She, C. Y., et al. (1995), Vertical structure of the mid-latitude temperature from stratosphere to mesopause (30–105 km), *Geophys. Res. Lett.*, *22*, 377–380, doi:10.1029/95GL00010.

She, C. Y., et al. (2002), Tides in the mesopause region over Fort Collins, CO (41°N, 105°W) based on lidar temperature observations covering full diurnal cycles, *J. Geophys. Res.*, *107*(D18), 4350, doi:10.1029/2001JD001189.

She, C. Y., et al. (2004), Tidal perturbations and variability in the mesopause region over Fort Collins, CO (41N, 105W): Continuous multi-day temperature and wind lidar observations, *Geophys. Res. Lett.*, *31*, L24111, doi:10.1029/2004GL021165.

Smith, A. K., D. V. Pancheva, N. J. Mitchell, D. R. Marsh, and M. G. Mlynczak (2007), A link between variability of the semidiurnal tide and planetary waves in the opposite hemisphere, *Geophys. Res. Lett.*, *34*, L07809, doi:10.1029/2006GL028929.

States, R. J., and C. S. Gardner (2000), Temperature structure of the mesopause region (80–105 km) at 40 N latitude: 2. Diurnal variations, *J. Atmos. Sci.*, *57*, 78–92, doi:10.1175/1520-0469(2000)057<0078:TSOTMR>2.0.CO;2.

Thomas, R. J. (1990), Seasonal ozone variations in the upper mesosphere, *J. Geophys. Res.*, *95*(D6), 7395–7401, doi:10.1029/JD095iD06p07395.

Tsuda, T., et al. (1988), Characteristics of semidiurnal tides observed by the Kyoto meteor radar and Saskatoon medium-frequency radar, *J. Geophys. Res.*, *93*, 7027–7036, doi:10.1029/JD093iD06p07027.

Tsutsumi, M., T. Tsuda, T. Nakamura, and S. Fukao (1996), Wind velocity and temperature fluctuations due to a 2-day wave observed with radio meteor echoes, *J. Geophys. Res.*, *101*, 9425–9432, doi:10.1029/95JD03579.

Vincent, R. A., T. Tsuda, and S. Kato (1989), Asymmetries in mesospheric tidal structure, *J. Atmos. Terr. Phys.*, *51*, 609–616, doi:10.1016/0021-9169(89)90058-5.

Walterscheid, R. L. (1981), Inertio-gravity wave induced accelerations of mean flow having an imposed periodic component: Implications on tidal

observations in the meteor region, *J. Geophys. Res.*, *86*, 9698–9706, doi:10.1029/JC086iC10p09698.

Walterscheid, R. L., J. G. DeVore, and S. V. Venkateswaran (1980), Influence of mean zonal motion and meridional temperature gradients on solar semidiurnal atmospheric tide: A revised spectral study with improved heating rates, *J. Atmos. Sci.*, *37*, 455–470, doi:10.1175/1520-0469(1980)037<0455:IOMZMA>2.0.CO;2.

Williams, B. P., R. G. Roble, and C. Y. She (1998), Seasonal climatology of the nighttime tidal perturbation of temperature in the midlatitude mesopause region, *Geophys. Res. Lett.*, *25*(17), 3301–3304, doi:10.1029/98GL02558.

Yu, J. R., J. States, S. J. Franke, C. S. Gardner, and M. E. Hagan (1997), Observations of tidal temperature and wind perturbations in the mesopause region above Urbana, IL (40°N, 88°W), *Geophys. Res. Lett.*, *24*, 1207–1210, doi:10.1029/97GL01023.

Yuan, T. (2004), Seasonal variations of diurnal and semidiurnal perturbations in mesopause region temperature and zonal and meridional winds above Ft. Collins, CO (40°N, 105°W) based on Na-Lidar observation over full diurnal cycles, Ph.D. dissertation, Colo. State Univ., Fort Collins.

Yuan, T., et al. (2006), Seasonal variation of diurnal perturbations in mesopause-region temperature, zonal, and meridional winds above Fort Collins, CO (40.6°N, 105°W), *J. Geophys. Res.*, *111*, D06103, doi:10.1029/2004JD005486.

Yuan, T., C.-Y. She, D. A. Krueger, F. Sassi, R. Garcia, R. G. Roble, H.-L. Liu, and H. Schmidt (2008), Climatology of mesopause region temperature, zonal wind, and meridional wind over Fort Collins, Colorado (41°N, 105°W), and comparison with model simulations, *J. Geophys. Res.*, *113*, D03105, doi:10.1029/2007JD008697.

D. A. Krueger, C. Y. She, and T. Yuan, Department of Physics, Colorado State University, Fort Collins, CO 80523, USA. (titus@lamar.colostate.edu)

S. Reising, Department of Electrical and Computer Engineering, Colorado State University, Fort Collins, CO 80523, USA.

H. Schmidt, Max Planck Institute for Meteorology, Bundestrasse 53, D-20146 Hamburg, Germany.